SAND2022-13454C

Detection and Localization of GPS Interference Source Based on Clock Signatures

Joseph B. Smith, Auburn University
Joshua M. Wood, Auburn University
Scott M. Martin, Auburn University
Connor Brashar, Sandia National Laboratories

Biographies

Joseph Smith is a Masters student in the GPS and Vehicle Dynamics Lab (GAVLAB) at Auburn University. He received his B.S. in Mechanical Engineering in 2018. His research interests include timing and inauthentic signal detection and localization.

Joshua Wood is a former graduate student at the Auburn University GPS and Vehicle Dynamics Laboratory. He received his Masters of Science in Mechanical Engineering in 2021. His research interests include GNSS assurance and the benefits of precise time for navigation.

Scott Martin is an Assistant Professor in the GPS and Vehicle Dynamic Laboratory at Auburn University. He received his PhD. and M.S. in Mechanical Engineering from Auburn University in 2017 and 2011 respectively and his B.S. in Systems Engineering from East Carolina University in 2008.

Connor Brashar has 8+ years experience in navigation warfare, GPS signal processing, and sensor fusion. He is currently a Senior Electrical Engineer at Sandia Laboratories, where he is a technical lead for Sandia's GPS-Denied Research Imperative. He leads several projects in GPS-contested navigation technologies.

Abstract

This paper focuses on the development and testing of spoofing detection and localization techniques that rely only on clock deviations to identify threat signals. Detection methods that rely on dynamic receiver geometries to triangulate threat locations or signal geometry to identify spoofing are not considered here. Instead this paper focuses on single antenna receivers and assumes the receiver tracks only the inauthentic signal. The quality of the receiver clock has a significant impact on the performance of the receiver tracking loops. Low quality clocks have frequency instabilities that inherently limit the sensitivity of the receiver to slow growing errors. Some clocks provide better frequency stabilities but have a higher white frequency noise that can induce false detections. Because of these trends, various detection methods are tested with four types of receiver and transmitter clocks of varying quality.

I. INTRODUCTION

The Global Positioning System (GPS) has long been used for providing an affordable and accurate position solution in applications ranging from autonomous vehicles to fleet tracking. The design of GPS satellites and the use of highly stable atomic clocks resulted in GPS Time (GPST) becoming a standard reference for various communication systems. As GPS and other Global Navigation Satellite Systems (GNSS) become more commonplace, methods for denying use have evolved. A combination of jamming and spoofing can disrupt operation of GPS receivers by obscuring satellite signals and replacing them with inauthentic signals. Two recent incidents of large scale spoofing are the Black Sea incident (Jones 2017) and crop circle spoofer threats (Harris 2019). Various research groups have worked on methods to detect and mitigate the effects of jamming and spoofing on GPS receivers using methods such as advanced antennas (Bitner et al., 2015), signal quality monitoring (SQM) (Miralles et al., 2020), or multisensory integration techniques (Tanil et al., 2018). Once a spoofing attack has been detected, it can be further mitigated if the source of the inauthentic signal is localized. This paper is a continuation of a research effort that was first presented at ION JNC 2021 (Smith et al., 2021).

II. MODELING AND CLOCK ESTIMATION

A two state clock model is used to simulate clock bias and clock drift for both the receiver clock and the inauthentic signal transmitter clock. The two states are simulated using the state space equation below:

$$\begin{bmatrix}\dot{b}\\ \ddot{b}\end{bmatrix} = \begin{bmatrix}0 & 1\\ 0 & 0\end{bmatrix}\begin{bmatrix}b\\ \dot{b}\end{bmatrix} + \begin{bmatrix}1 & 0\\ 0 & 1\end{bmatrix}\begin{bmatrix}w_b\\ w_r\end{bmatrix} \quad (1)$$

The process noise parameters are based on the white frequency modulation (H_0) and the random walk frequency modulation (H_{-2}) characteristics of the specified clock. The Kalman filter process noise matrix is calculated as shown in Equation (2).

$$Q_{clk} = \begin{bmatrix}\frac{H_0}{2}T + \frac{2\pi^2 H_{-2}}{3}T^3 & \frac{2\pi^2 H_{-2}}{2}T^2\\ \frac{2\pi^2 H_{-2}}{2}T^2 & 2\pi^2 H_{-2}T\end{bmatrix} \quad (2)$$

Four types of receiver and transmitter clocks were used in this research including two crystal oscillators and two rubidium clocks. Table 1 containing the clocks used in this study and their associated power law coefficients is provided below (Brown & Hwang 2012).

Table 1: Receiver Clocks and Power Law Coefficients

Clock Type	White FM (H_0)	Random Walk FM (H_{-2})
TCXO	2.8e-23	2.4e-23
OCXO	2.2e-25	1.6e-24
CSAC	1.8e-19	5.36e-29
Rubidium	2.0e-22	1.0e-30

The TCXO (Temperature Compensated Crystal Oscillator) and OCXO (Oven Controlled Crystal Oscillator) both use a crystal oscillator to generate a timing signature but use different methods to compensate for errors caused by temperature fluctuations. The TCXO measures the temperature and scales the oscillator power accordingly and is less accurate than an OCXO. The OCXO places the oscillator in an oven to keep it at a constant temperature. The two atomic clocks (e.g. Rubidium and CSAC) use a physics package to keep a stable frequency reference. The CSAC (Chip Scale Atomic Clock) is a miniaturized package that is more versatile at the cost of performance. The performance of these clocks can be described in the time domain using an Allan deviation plot. The Allan deviation or Allan variance (Allan deviation squared) is a common statistic used to summarize an oscillator's performance with respect to sampling times. The Allan deviations for the clocks described in Table 1 ares shown in Figure 1 below.

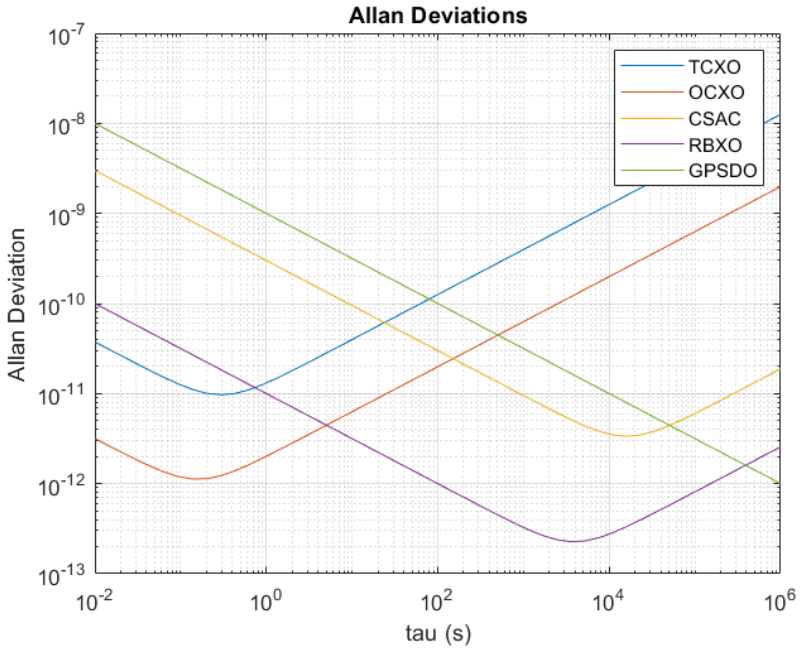

Figure 1: Allan Deviation for Clocks of Varying Qualities

The relative performance of a crystal oscillator is better over the short term because of lower Allan deviations at shorter sampling times as shown by the quartz oscillator in Figure 1. The benefit of an atomic clock is the long term stability as shown by the decreasing Allan deviation with respect to averaging time for both the CSAC and rubidium. Lastly a GPS disciplined oscillator (GPSDO) is referenced to show the Allan deviation for a clock that is corrected over time and therefore has no long term random walk. In general, atomic clocks have relatively higher frequency noise and better long-term stability. The two crystal oscillators have less frequency noise but are more likely to have noticeable random walk.

The carrier phase measurement is the most precise measurement generated by the GPS receiver. The received phase can often be measured to 2mm and is a great resource to detect anomalies in the received signal. Atmospheric delays corrupt the carrier phase measurement, and the integer ambiguity is an unknown bias in the measurement. One approach to mitigating the measurement errors is to compute the time difference carrier phase measurement. The atmospheric delays are nearly constant over a short time period resulting in a measurement that can be used for precise estimation of the receiver clock drift. The model for time difference carrier phase is shown below as a function of the receiver clock error (cdt_A) , and satellite clock error (cdt^m).

$$\Delta\phi_{A_{k-\tau,k}}^{m_{k-\tau,k}} = r_{A_{k-\tau,k}}^{m_{k-\tau,k}} + cdt_{A_{k-\tau,k}} - cdt_{k-\tau,k}^{m} + \varepsilon_{A_{k-\tau,k}}^{m_{k-\tau,k}} \tag{3}$$

In the equation, $r_{A_{k-\tau,k}}^{m_{k-\tau,k}}$ is the change in range from receiver to satellite over the differencing window and $\varepsilon_{A_{k-\tau,k}}^{m_{k-\tau,k}}$ is assumed to be additive Gaussian white noise.

Satellite clock drift is predictable using clock parameters broadcast by the satellites. A velocity and clock drift Kalman filter was developed to evaluate the impact of an inauthentic signal on a receiver. The noise value used for the carrier phase measurement is modeled as a zero mean Gaussian white noise with variance dependent upon the carrier-to-noise ratio, as shown in the equation below.

$$\sigma_{\varepsilon}^{2} = \frac{2\pi^2\lambda_{L1}^2}{T\frac{C}{N_0}} \tag{4}$$

III. INAUTHENTIC SIGNAL DETECTION

Detection of the inauthentic signal is performed using Kalman filter estimates of the clock states and the normalized residuals. Three different methods were tested for detection using both clock bias and clock drift residuals including innovation filtering, innovation sequence monitoring, and a multiple receiver residual variance. Innovation filtering and innovation sequence monitoring are standard fault detection methods for Kalman filters being applied to clock states. Innovation filtering determines if the most recent measurement is consistent with previous measurements and compares the magnitude to a threshold value. The threshold is related to a Gaussian distribution, therefore a value of three implies that 99.7% of authentic measurements will not cause a fault. The equation representation is seen below (Groves 2013).

$$y_k = \left| \frac{\delta z_k}{\sqrt{C_{\delta z_k}}} \right| > 3 \tag{5}$$

Innovation sequence monitoring uses normalized innovations to find slow growing errors using the average innovation over the previous N measurements. This average is compared to a threshold value normalized by square root of the number of samples (Groves 2013).

$$\mu_k = \frac{1}{N} \sum_{i=k+1-N}^{k} y_i \tag{6}$$

$$|\mu_k| > \frac{T}{\sqrt{N}} \tag{7}$$

The third method evaluated is a multiple receiver residual variance detection that was derived to use networked receivers to detect an inauthentic signal. This method also uses the residuals from the filter but finds the variance of the individual satellite channel residuals, $\sigma^2_{\delta z_{k,rx}}$. This collection of variances is then compared to the innovation covariance, $C_{\delta z_k}$, for one of the receivers resulting in a unitless value. This unitless value is be compared to a threshold value. A fault occurs if the threshold value TS is exceeded.

$$\sigma^2_{\delta z_{k,rx}} = \frac{1}{k}\sum_{i=1}^{k} E_i\left[(\delta z_{i,rx} - \delta \bar{z}_{i,rx})^2\right] \tag{8}$$

$$\frac{\sigma^2_{\delta z_{k,rx}}}{C_{\delta z_k}} > \text{TS} \tag{9}$$

1. Simulation Scenario

The initial simulated scenario takes place in three phases. First the receivers receive authentic GPS signals to get an initial position solution and start the Kalman filter estimates. Then the receivers are denied any signal to represent a jamming interference. Then in the third phase the receiver is only tracking the inauthentic signal. The initial results are all for a group of five static receivers. A dynamic simulation and results are discussed in a later section. Detection results are geometry independent but the receivers are approximately 100-meters away from the transmitter for these results.

2. Simulation Results

The criteria used to evaluate the fault detection testing are a fault detected percentage and a false detections percentage. An accurate fault detection is any fault detection in the third phase during inauthentic signal reception. A false detection is any fault detection during the first period of the simulation when the true GPS signal is present. Figure 2 shows a comparison of the residuals for a single receiver that goes back to an authentic GPS signal on the left versus an inauthentic signal on the right. The innovation filtering looks for a majority of the channel residuals to be outside of the three sigma bounds at any instant, or a constant shift of the residuals for innovation sequence monitoring.

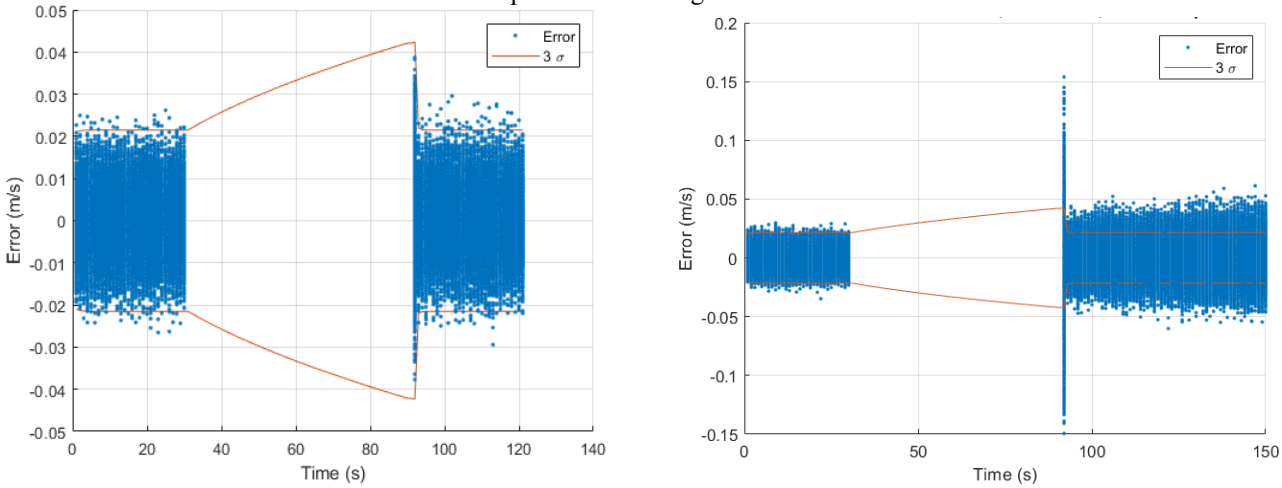

Figure 2: Single Receiver Residuals Comparison After Outage, Clean Left and Inauthentic Right

The multiple residual variance detection method can be visualized by plotting a moving mean of the residuals overtime. In Figure 3 below, the moving mean is calculated before and after the outage period. The large spike immediately after the outage is due clock dead reckoning during the entire outage. The initial spike also occurs when the receiver re-locks on the authentic signal after an outage. Accordingly, the first measurement is neglected. After the initial spike, the moving mean settles to a value above original residual variance. This notable increase was the motivation to develop the multiple residual variance detection method.

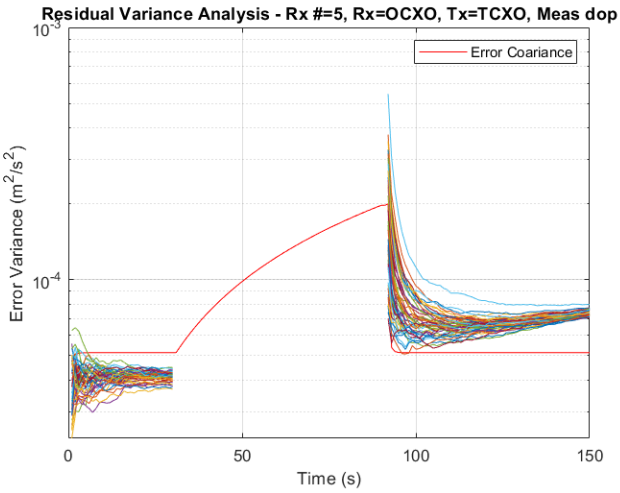

Figure 3: Multiple Receiver Variance Moving Mean

3. Generalized Results

The simulations showed that higher quality clocks result in higher detection rates and less false detections. The clocks with larger frequency noise terms tended to be easier to detect, including the CSAC. The innovation sequence monitoring was the worst method evaluated with equal or less detection rates at the cost of higher false detections. The multiple receiver detection method was the best method with 100% detections for all clocks except the TCXO. Similarly, no false detections occurred except for with the TCXO. Once the detection methods had been evaluated, they were incorporated into the range estimation and localization algorithm. More complete results are available in a previous publication on this research in Smith et al (2021).

IV. INAUTHENTIC SIGNAL DETECTION HARDWARE VALIDATION

The inauthentic signal detection algorithms were verified using hardware in the loop (HWIL) testing with a record and playback setup to mimic an environment with an inauthentic signal. To create the environment, two RF signals were recorded using a software defined radio (SDR). One signal acts as the truth data. The second is the inauthentic signal recorded simultaneously. The recorded signals are mixed using a record and playback setup consisting of three SDR's, (two for playback and one to record). A programmable attenuator box is used to control when the signals are passed to the recorder. The inauthentic signal is delayed to account for the transit time between receiver and transmitter. An example schematic of the HWIL setup is shown in Figure 4. The receiver clock under test is used to sample of the truth signal and the combined signal. A secondary clock can be used to feed the transmitter clock if desired. The HWIL results published in this paper includes 5 receivers in the same environment receiving the same inauthentic signal to run the multiple receiver variance detection algorithm.

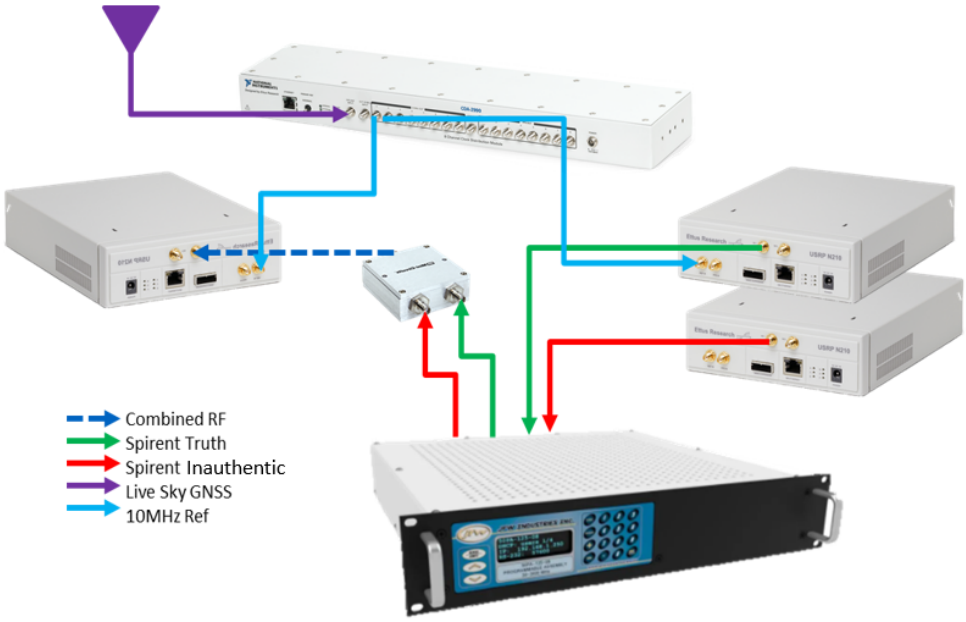

Figure 4: Hardware in the Loop Test Setup

The following HWIL results are from a data set using a GPSDO as the reference oscillator as shown in Figure 4. The first result plot, Figure 5, shows the innovation filtering results for all five receivers as a binary fault indication. Both clock bias and clock drift residuals are evaluated. The clock bias performed poorly with two of the five receivers giving false alarms during normal operation (shown in red). All receivers detected the fault within 40 seconds of tracking the inauthentic signal, which includes time to acquire the new signal. Clock drift detection outperformed the clock bias detection with only one receiver having a single false detection instance and all five receivers detected the inauthentic signal. However, the clock drift does not have a consistent positive fault detected, with some receivers going in and out of being faulted.

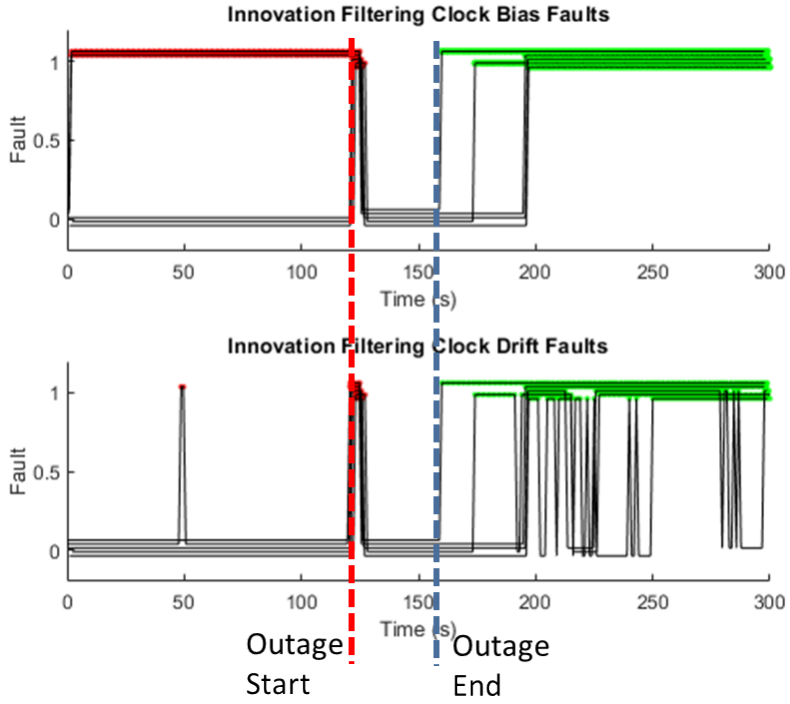

Figure 5: Innovation Filtering HWIL Results

As shown in Figure 6, the multiple receiver variance detection method performed better than the innovation filtering with a consistent innovation value well over the threshold value and only one false detection at the same time as the innovation filtering example around time 50 seconds. These results show the two methods that performed best in simulation could work using realistic signal data.

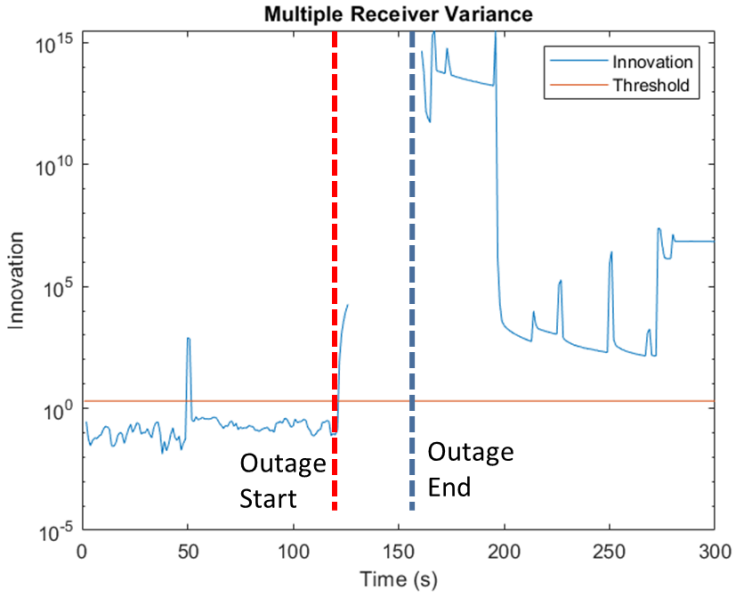

Figure 6: Multiple Receiver Variance HWIL Results

V. RANGE ESTIMATION

Range is estimated by taking the difference between the true receiver clock bias and the receiver clock bias after the inauthentic signal captures the receiver. This research assumes the receiver cannot track both the authentic and inauthentic signals, and the receiver cannot observe the true receiver clock bias. Instead, the clock bias is dead reckoned during the outage period propagated forward while holding the clock drift constant. Dead reckoning the clock states results in a clock bias error that affects range estimation accuracy and is related to quality of oscillator used and duration of the signal outage.

The algorithm developed operates as a single state vector, known as the receiver state, while running under normal operation. Once a fault is detected a second state vector, referred to as the capture state, is started and tracks the inauthentic signal. The original state vector is reset to the last known safe measurement and dead reckons the clock states forward to the current measurement, then the capture state continues to estimates clock bias and clock drift using the inauthentic signal while accounting for the dead reckoned terms. The capture state clock bias, which accounts for the dead reckoned receiver clock bias, is used as the range estimate. This range estimate, b_{sp}, is assumed to be a combination of the range between the receiver and transmitter as well as a bias term that affects all receivers equally. A mathematical explanation of how the algorithm works is shown below in Equations (10-11).

$$\rho_{GPS} = r_{rx}^{sv} + b_{dr} + b_{sp} + b_{sv} + \eta \tag{10}$$

$$b_{sp} = r_{tx}^{rx} + b_{tx} \tag{11}$$

The new range measurement from the inauthentic signal includes a known dead reckoned bias, b_{dr}, the known satellite clock bias, the true range which is estimated, and an additional bias term, b_{sp} which is the estimated as the capture state clock bias. All other non-clock error terms are summarized by η.

VI. LOCALIZATION OF INAUTHENTIC SIGNAL SOURCE

The localization portion of the algorithm uses an iterative least squares (LS) position estimator to localize the transmitter of the inauthentic signal. This algorithm uses the estimated ranges to calculate four states including the three-dimensional transmitter position in the ECEF coordinate frame, and a clock bias/propagation delay that is consistent with the estimated

ranges for all receivers. Unlike with GPS where satellites are often distributed above the receiver, using a group of receivers to locate a transmitter may lead to a wide variety of geometries and extra steps are needed to get consistent localization. Due to the varying geometries when localizing an inauthentic signal source an accurate initial estimate is needed as described by Wang et al (2021). An initial estimate filter is used to find a suitable initial position that can then be improved upon using the iterative LS. Another difficulty in localizing using a group of receivers is the geometric observability summarized by the geometric dilution of precision (GDOP). The relative transmitter location with respect to receiver locations can cause the estimator to develop a vector in which a change in bias estimate results in a proportional change in position while affecting all ranges equally creating a vector of transmitter estimates. The vector of estimates is referred to as the uncertainty vector in this paper and will be shown visually in the next section.

1. Initial Estimate Filter

The initial filter estimate is intended to get an accurate enough position estimate that the LS will be able to converge to a solution. Both a deterministic and random sampling approach were evaluated for the initial filter. Both filter methods use one receiver to act as the central receiver then generate samples points to test with the cost function.

The first filter method evaluated deterministic sampled points that encircle the chosen receiver at various azimuth angles, then create another set of samples at the best azimuth angle varying altitude angles. The radius between the receiver and samples is equal to the range estimate for the central receiver and are spaced apart by one degree of azimuth. The second sampling method is a random distribution of points that are spaced using a Gaussian distribution with the one standard deviation being equivalent to the range estimate. The best random sample is then used at the center point for a second distribution of random samples, but with a 10-meter standard deviation to try and improve the initial estimate.

Both filter methods were tested with two different cost functions that use range errors. The first cost function is a minimal mean for range errors and the second solves for the minimal variance of range errors. The minimal mean attempts to find the position that has the lowest errors but does not have any consideration for the potential bias that affects all range estimates equally, similar to how receiver clock bias affects GPS pseudoranges. Figure 7 below shows the two components of the range estimate.

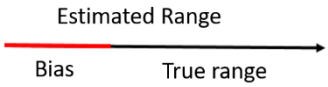

Figure 7: Estimated Range Components

The minimal variance was created after simulation testing with the minimal mean cost function would result in multiple solutions with a similar cost or an inaccurate solution. A minimal variance for range errors intends to account for the range bias indirectly by finding the position estimate where all range errors are close to equal. The consistent error across all ranges is a rough estimate of the actual bias that affects the range estimates. A visual comparison of the two methods is shown below in Figure 8 using the same color scheme as Figure 7.

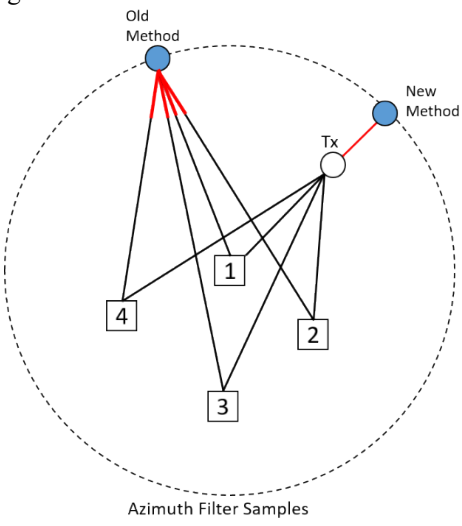

Figure 8: Initial Estimate Filter Cost Function Comparison

2. Least Squares Position Estimator

Once the initial position is estimated, the LS estimator attempts to improve the transmitter position estimate. Equation (12) shows how the unit vectors between the receivers and the transmitter to be located are calculated using receiver position r_i and the initial transmitter estimate from the initial filter tx.

$$\mathbf{1}^{(i)} = \begin{bmatrix} \frac{x_r - x_{tx}}{\|r_i - tx\|} \\ \frac{y_r - y_{tx}}{\|r_i - tx\|} \\ \frac{z_r - z_{tx}}{\|r_i - tx\|} \end{bmatrix} \tag{12}$$

The unit vectors between receivers and transmitters are used to create the geometry matrix G as well as an estimated range that is subtracted from the measured range $\tilde{\rho}$ to linearize about that point.

$$G = \begin{bmatrix} (-\mathbf{1}^{(1)})^T & 1 \\ (-\mathbf{1}^{(2)})^T & 1 \\ \vdots & \vdots \\ (-\mathbf{1}^{(k)})^T & 1 \end{bmatrix}, \Delta\rho = \tilde{\rho} - (\|r_i - tx\| + b) \tag{13}$$

The geometry matrix and delta range estimate are then used to get a LS solution with delta terms that are used to shift the transmitter estimated position.

$$\begin{bmatrix} \Delta x_{tx} \\ \Delta y_{tx} \\ \Delta z_{tx} \\ \Delta b \end{bmatrix} = (G^T G)^{-1} G^T \Delta p \tag{14}$$

The iterative LS repeats Equations (12-14) using the updated transmitter position until the current and previous estimates are less than 1-meter apart.

3. Uncertainty Vector

The uncertainty vector is used to summarize the degradation of estimator performance due to the relative geometry between the transmitter and the receivers. The direction of the uncertainty vector is based on the geometry matrix and GDOP. For most instances where the transmitter is outside of the group of receivers, the uncertainty vector acts as a line of bearing between the receivers and transmitter. For scenarios where the transmitter is within a group of receivers, the uncertainty vector is in the altitude direction unless there is enough altitude variance amongst the receivers. The math to calculate the GDOP and find the direction of the uncertainty vector uses the geometry matrix.

$$H = (G^T G)^{-1} = \begin{bmatrix} \sigma_x^2 & \sigma_{xy}^2 & \sigma_{xz}^2 & \boldsymbol{\sigma_{xb}^2} \\ \sigma_{xy}^2 & \sigma_y^2 & \sigma_{yz}^2 & \boldsymbol{\sigma_{yb}^2} \\ \sigma_{xz}^2 & \sigma_{yz}^2 & \sigma_z^2 & \boldsymbol{\sigma_{zb}^2} \\ \boldsymbol{\sigma_{xb}^2} & \boldsymbol{\sigma_{yb}^2} & \boldsymbol{\sigma_{zb}^2} & \sigma_b^2 \end{bmatrix} \tag{15}$$

The bolded terms in equation 15 are used to find the direction of the uncertainty vector. The unit vector for the uncertainty vector can be solved for using equation 16.

$$u = \frac{1}{\left\|\sigma_{xb}^2 + \sigma_{yb}^2 + \sigma_{zb}^2\right\|} \begin{bmatrix} \sigma_{xb}^2, & \sigma_{yb}^2, & \sigma_{zb}^2 \end{bmatrix}^T \tag{16}$$

VII. LOCALIZER RESULTS

The simulation scenario involves four receivers in a square shape measuring 50-meters across diagonally with a 5th receiver located 50-meters above the center of the square to form a pyramid. All receivers use the same quality of clock. The transmitter is located approximately 500-meters southwest of the group of receivers. The Monte Carlo simulation includes 50 simulation runs and multiple estimates per simulation.

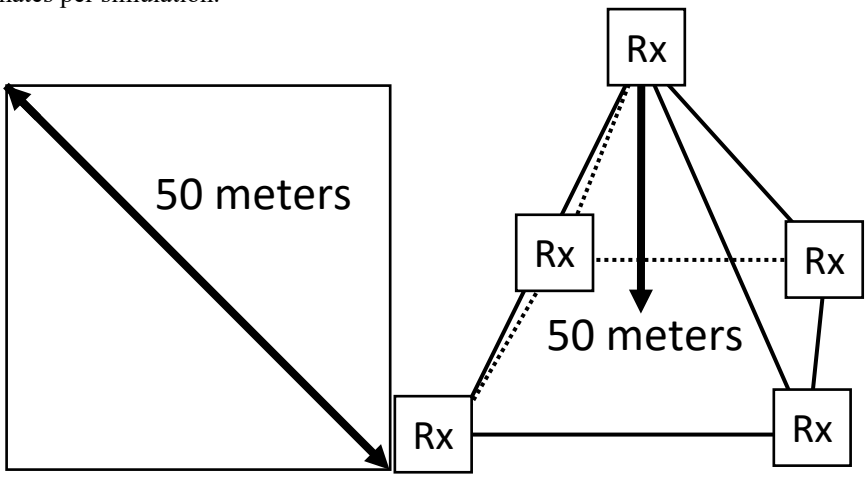

Figure 9: Static Scenario Receiver Geometry

From testing the algorithm, three different state vectors have been used to estimate the transmitter location. All use the same LS method, initial estimate, receiver position, and range estimates but vary the state vector estimated. The three state vectors are the original four-state ECEF position with a bias estimate as the fourth state described previously, a three state ECEF position with no bias, and a three-state vector that estimates a North, East, and bias value. The different localizer state vectors and their performance is discussed in the next section.

The four-state localizer, referred to as the 3D localizer, is designed to both localize the transmitter and remove any bias that may be on all of the range estimates. In testing it had issues where the bias could increase or decrease and affect all ranges equally making it difficult to localize to an exact point. Instead, the estimates are distributed along the uncertainty vector as seen in the left plot of Figure 10.

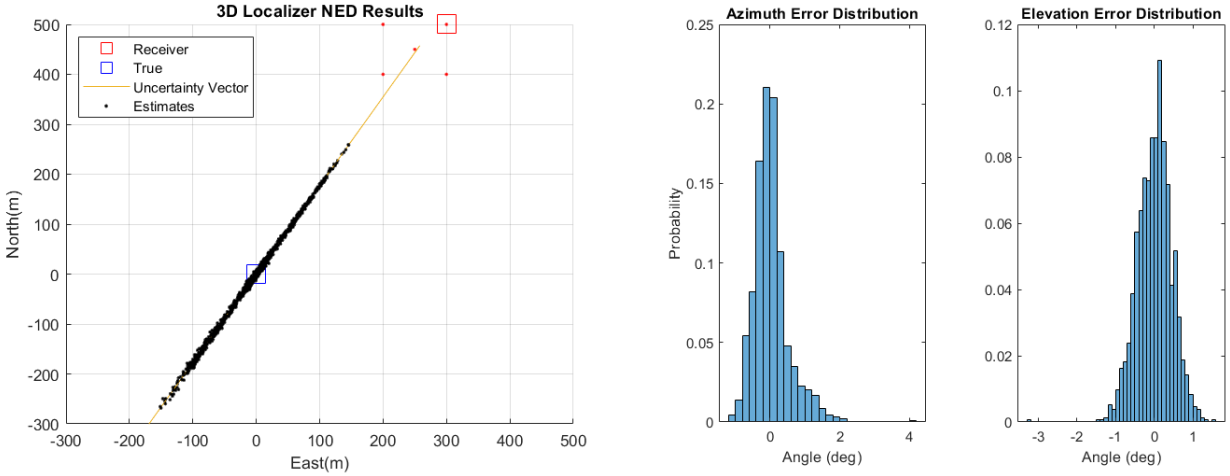

Figure 10: 3D Localizer Result (left) and Line of Bearing Error Histogram (right)

As seen in Figure 10, the estimates are all distributed along the uncertainty vector. When the transmitter is located far enough outside of the group of receivers the uncertainty vector can act as a line of bearing to the transmitter as shown by the histograms showing azimuth and elevation angle errors. The statistics for varying clock qualities and the associated azimuth and elevation angles are shown in Table 2.

Table 2: Line of Bearing Error Comparison Between Clocks

Clock	TCXO		OCXO		CSAC		Rubidium	
Angle	Azimuth	Elevation	Azimuth	Elevation	Azimuth	Elevation	Azimuth	Elevation
Mean	-0.8927	0.3367	0.1641	-0.0482	0.0746	0.3234	-0.0318	0.01
Std. Dev.	2.3404	4.3659	1.537	2.3623	1.3073	1.7065	0.5012	0.4441

The second state vector evaluated is intended to reduce the error along the uncertainty vector. To remove this error source, the bias estimate is removed and only the three ECEF coordinates are estimated. This method can improve results but is susceptible to passing on range errors into the localization errors. However, for the same set of ranges used in the 3D localizer the no bias estimator performed better as shown below in Figure 11.

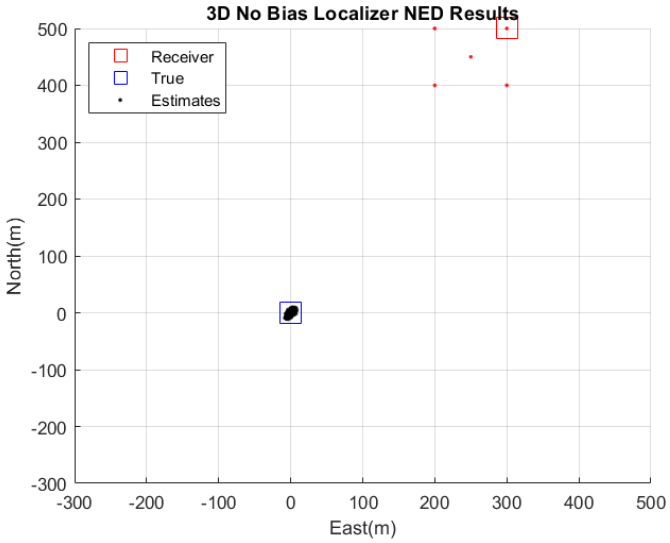

Figure 11: 3D Localizer with No Bias Estimate Results

The last state vector is the 2D localizer that only evaluates values at a set altitude aligned with the receivers. This method is more beneficial when the receivers are all at the same altitude with no geometric observability for altitude changes. The 2D localizer slightly improves the results but still suffers from the uncertainty vector to a lesser degree.

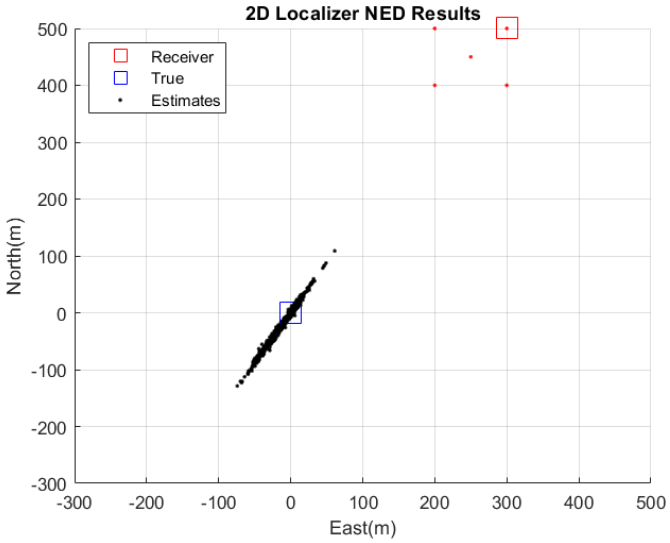

Figure 12: 2D Localizer Results

VIII. DYNAMIC SCENARIO SIMULATION

Initial algorithm development and testing was performed using a group of static receivers as described in the previous sections. This section will describe the adaptation of the algorithm to accommodate for dynamic receivers. Having a dynamic receiver brings in new sources of error that need to be addressed. The new error sources include unknown receiver position during outage periods and when tracking the inauthentic signal as well as increased oscillator frequency noise due to acceleration. The unknown receiver position is addressed by using an inertial navigation system (INS) to maintain a position solution that can be used for localization. The dynamic algorithm uses an error state Kalman filter to estimate gyro and accelerometer biases to improve the INS performance when GPS is no longer available or trusted. The dynamic scenario tested involves a single receiver travelling in a 100-meter radius circle with the transmitter in the center of the circle at the same altitude and takes one minute to complete a rotation about the transmitter.

Below are results for the three localizer methods using the same ranges and positions. Unlike the static case, some localization errors occurred due to the position error from the INS propagating without any corrections from GPS during the outage. This is especially important when looking at the 2D localizer because the altitude error is solely caused by the INS altitude error.

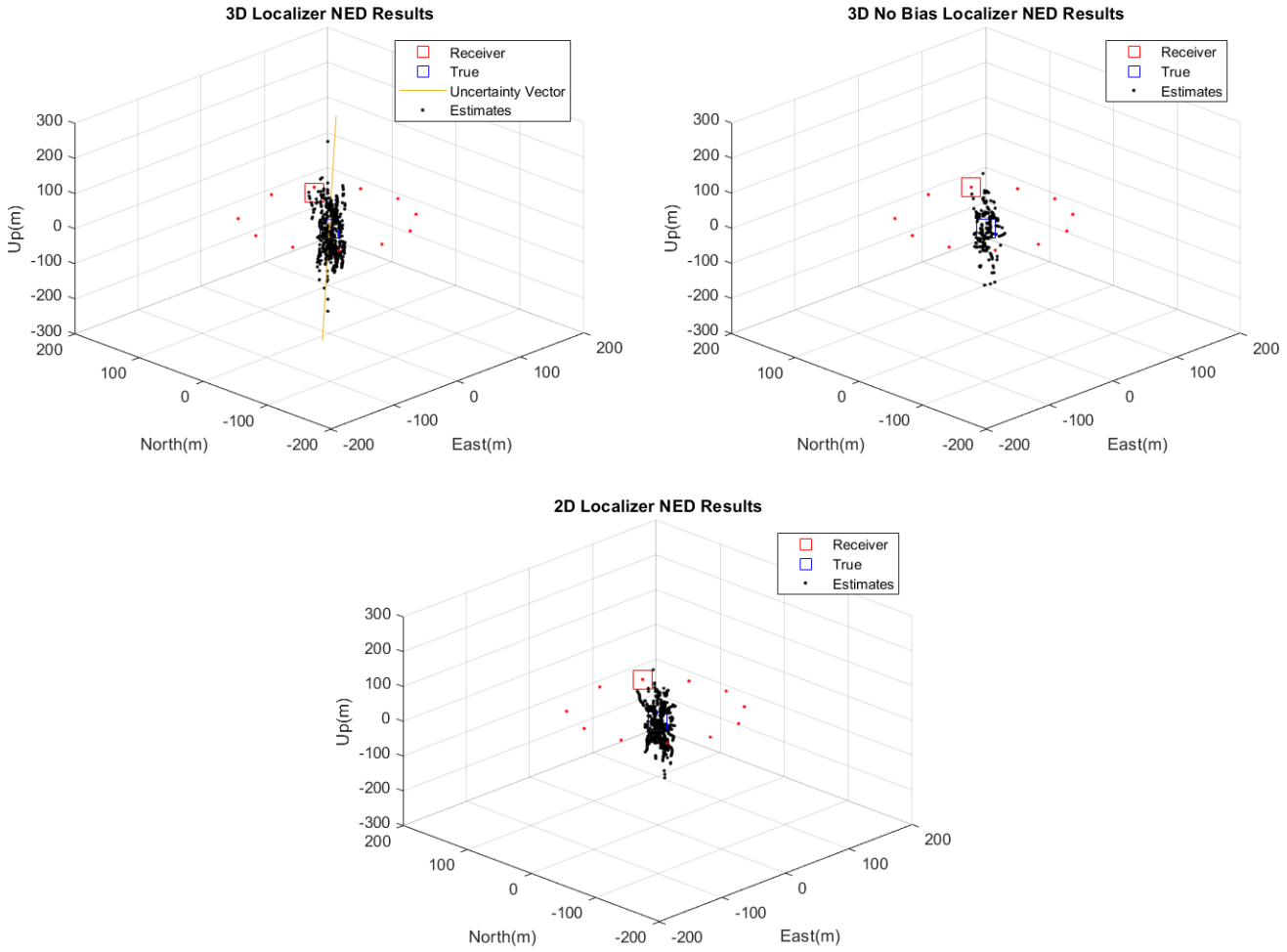

Figure 13: Dynamic Scenario Results for 3D (top left), No Bias (top right), and 2D (bottom) Localizers

The uncertainty vector shown in the top left plot of Figure 13 is mostly aligned with the altitude axis and is almost perpendicular to the plane created by the receivers. Similar to the static scenario, the estimates are distributed along the uncertainty vector. Of the three localization methods, the 3D and 2D localizers had the best performance. Any bias would be common to all measurements because a single receiver is used. Note that the down error on the 2D localizer is caused solely by the INS position errors caused by an unmeasured pitch offset.

IX. CONCLUSIONS

This paper discusses the feasibility of detecting and localizing the source of an inauthentic signal using only clock based methods and measurements. The use of a receiver clock and receiver clock model is shown to be effective in detecting an inauthentic signal with both innovation filtering and multiple receiver variance. These detection algorithms were verified using hardware in the loop tests. Some of the difficulties of localization are discussed and methods are provided to mitigate error sources such as the initial estimate filter. With an accurate initial estimate, a least squares localizer is able to give an accurate transmitter location depending on the geometry and dilution of precision.

The research shared in this report is from an ongoing research project sponsored and funded by Sandia National Laboratories. Sandia National Laboratories is a multi-mission laboratory managed and operated by National Technology & Engineering Solutions of Sandia, LLC, a wholly owned subsidiary of Honeywell International Inc., for the U.S. Department of Energy's National Nuclear Security Administration under contract DE-NA0003525.

This paper describes objective technical results and analysis. Any subjective views or opinions that might be expressed in the paper do not necessarily represent the views of the U.S. Department of Energy or the United States Government.

REFERENCES

Bitner, T., Preston, S., & Bevly, D., Multipath and Spoofing Detection Using Angle of Arrival in a Multi-Antenna System. *Proceedings of the 2015 International Technical Meeting of The Institute of Navigation (ION ITM 2015)*, Dana Point, CA, 822-832.

Brown, R. G., & Hwang, P. Y. C. (2012). Introduction to random signals and Applied Kalman filtering with Matlab exercises, 4th edition. *John Wiley & Sons*.

Fernández, E., Calero, D., & Parés, M. (2017). CSAC Characterization and Its Impact on GNSS Clock Augmentation Performance. *Sensors*, *17*(2), 370. https://doi.org/10.3390/s17020370

Groves, P. D. (2013). Principles of GNSS, Inertial, and Multisensor Integrated Navigation Systems. United Kingdom: Artech House.

Miralles, D., Levigne, N., Bornot, A., Rouqette, P., Akos, D., Chen, Y., Lo, S., & Walter, T. (2020) Assessment of GPS Spoofing Detection via Radio Power and Signal Quality Monitoring for Aviation Safety Operations. *IEEE Intelligent Transportation Systems Magazine, GNSS ITS,* 136-146. doi: 10.1109/MITS.2020.2994117.

Smith, J. B., Wood, J., Martin, S., & Brashar, C., (2021). Detection and Localization of an Adversarial GPS Interference Source Based on Clock Signatures. *Proc. of the 2021 Joint Navigation Conference of the Institute of Navigation (ION JNC 2021), Covington, KY,* 908-928.

Tanil, C., Khanafseh, S., Joerger, M., & Pervan, B. (2018) An INS Monitor to Detect GNSS Spoofers Capable of Tracking Vehicle Position. *In IEEE Transactions on Aerospace and Electronic Systems,* 131-143. doi: 10.1109/TAES.2017.2739924.

Wang, Z., Li, H., & Wen, J., Lu, M. (2021). Prototype Development of an Online Spoofer Localization System Using Raw GNSS Measurements of Android Smartphones, *Proceedings of the 34th International Technical Meeting of the Satellite Division of The Institute of Navigation (ION GNSS+ 2021)*, 1989-1999. https://doi.org/10.33012/2021.17995